RSC Advances

PAPER

View Article Online
View Journal | View Issue

Cite this: *RSC Adv.*, 2021, **11**, 14276

Fabrication of porous polymer coating layers with selective wettability on filter papers *via* the breath figure method and their applications in oil/water separation†

Xu Zhang, [ac] Guangping Sun,*[a] Heng Liu*[b] and Xuequan Zhang[b]

A comb-like amphiphilic polymer (PBTF), composed of hydrophobic backbones and hydrophilic side chains, was employed to grow honeycomb coating layers *in situ* on a filter paper *via* directly casting a polymer solution and by the subsequent dynamic breath figure (BF) method. Through regulating the hydrophilic polymer side chain density and the solution concentration, a continuous honeycomb coating layer contouring to the filter paper surface profile, in addition to possessing a water contact angle (WCA) as high as 146°, was successfully fabricated. The present study also finds that increasing the hydrophilic side chain density will turn PBTF into a surfactant-like polymer, and thus, endow the PBTF solution with the capacity of numerous micro–nano-sized water droplets, rather than simply stabilizing the ordered water droplet arrays on the surface of the solution. With vast nano-sized water droplets in it, the once transparent PBTF solution changed into a translucent nano-emulsion, which demonstrates a strong Tyndall effect. While casting such nano-emulsion on a filter paper and then subjecting to the BF process, the polymeric solute takes both nano-emulsion intrinsic nano-sized water droplets and solvent evaporation-induced water droplets as templates and self-assembles into a bird-nest-like three-dimensional porous microstructure, which possesses micro–nano-sized communicating pores. By regulating the water content in the nano-emulsion, the bird-nest-like structure can be uniformly formed on the surface of the filter paper, which revealed a WCA of 152°. The coated filter papers possess selective wettability, and meanwhile, maintain the inherent permeability of the substrates, which therefore can be directly utilized as oil/water separation materials.

Received 8th February 2021
Accepted 28th March 2021

DOI: 10.1039/d1ra01080h

rsc.li/rsc-advances

Introduction

Breath figure (BF) refers to a commonly observed phenomenon that condensed water droplets spontaneously array orderly on a cold surface in humid atmosphere. The formation process of BF was first investigated by Lord Rayleigh in 1911 (ref. 1 and 2), and such a process was utilized to prepare polymeric porous membranes by François *et al.* in 1994.[3] In a typical BF process, a polymer first dissolves in highly volatile solvents, and then casts on a substrate in a highly humid environment. The water vapors gradually condense on the cold surface of the polymer solution as a result of the rapid evaporation of the volatile solvent. These condensed water droplets self-assemble into ordered arrays, which are then taken as the templates for pore generation. After the solvent and water are completely evaporated, an ultrathin membrane with honeycomb-like pores is left behind.[4–7] The unique advantages of the BF process including low cost, time-saving and facile implementation pave the way to fabricate an ordered porous polymeric membrane with high efficiency and the formed honeycomb membrane shows potential applications in sensing,[8,9] bio-engineering,[10,11] and selective separation.[12,13] Among these application fields, selective separation is of great interest due to the urgent environmental problem caused by oil spill accidents and industrial wastewater discharge. Since the selective separation is related to interfacial properties, designing permeable honeycomb

[a]*College of Materials Science and Engineering, Jilin University, Changchun 130022, People's Republic of China. E-mail: sungp@jlu.edu.cn*

[b]*Key Laboratory of Rubber-Plastics, Ministry of Education/Shandong Provincial Key Laboratory of Rubber-Plastics, Qingdao University of Science & Technology, Qingdao 266061, People's Republic of China. E-mail: hengliu@qust.edu.cn*

[c]*College of Materials Science and Engineering, Jilin Jianzhu University, Changchun 130118, People's Republic of China. E-mail: xzhang@ciac.ac.cn*

† Electronic supplementary information (ESI) available: Fig. S1 shows the polymer solution droplets profile in water, Fig. S2 shows SEM image of deep furrow covered by honeycomb coating layer, Fig. S3 shows schematic view of a spherical water droplet at the air/solution interface, Fig. S4 shows SEM images of the coating layers formed by PBTP-30 by spin coating method on (a) filter paper; (b) planar glass slide. Fig. S5 shows the strong Tyndall effect displayed by N-50 under the 405 nm ultraviolet light, Fig. S6 shows the vertical direction SEM images of the coating layers by N-50 (5 mL, 10 mg mL^{-1}) with 2 μL water, Fig. S7 shows the water contact statue under the oil phase of the N-50 coated filter paper, eqn S1. The calculation equation of pore layers number formed by BF process, Video 1 shows the oil/water separation process, Video 2 shows the oil/water separation process, and the data provide by it was employed in flux calculate. See DOI: 10.1039/d1ra01080h

membranes with opposite wettabilities towards the oil/water phase is the key point of these kinds of studies. Until date, numerous polymers and polymer blends have been applied for the fabrication of honeycomb membranes with selective wettability.[14–18] The superhydrophobic surface shows better separation efficiency than that of the hydrophobic one, and hence, it is most desirable. However, the honeycomb membrane formed on the planar surface is generally too thin to afford enough mechanical strength required for large-area gravity-driven filtration. The composite filters composed of honeycomb membranes and porous substrates require a careful membrane transfer from the original planar substrate onto the porous support materials.[19–21] Previous studies have reported in the literature that self-supported monolithic membranes can be used as oil/water separation filters, which were prepared by a phase inversion method combined with the simultaneous breath figure method.[22–25] It still matters that the membrane is cracked or wrinkled in the process of transfer or use due to the brittleness caused by the inherent loose structure of the membrane. Furthermore, these self-supported membranes are raw materials consumed, which limit its mass-production. *In situ* generated permeable honeycomb membranes with selective wettability on porous substrates can effectively solve this problem. Bormashenko *et al.* fabricated a micro-scaled porous hydrophobic/oleophilic polycarbonate honeycomb membrane on a stainless steel gauze by the BF process. The separation efficiency of petroleum oil/water by this composite is 94%.[13] Zhang *et al.* constructed a well-defined porous texture from octadecyl-functionalized silica nanoparticles and polymethylmethacrylate (PMMA) on scaffolds of polyurethane sponges by the BF process. The composite realized the selective adsorption of oils and/or organic solvents from water, as well as the separation of oil/water mixtures. The separation efficiency toward HFE7500 oil is 85.7% (quantified by the mass ratio R (%)).[26] Guan *et al.* presented modified textiles using polystyrene (PS), PS-*block*-polybutadiene-*block*-PS (SBS), and asphalt as raw materials formed contouring to fiber surfaces of a fabric substrate as a three-dimensional (3D) conformal layer of porous microstructures by the BF self-assembling strategy. The composite with a modified hydrophobic surface can be utilized as a separation filter of oil/water mixtures.[27] The above-mentioned honeycomb membranes have shown hydrophobicity; however, when being introduced by low-surface-energy substances, for example, fluorine-containing, organosilanes or functionalised SiO_2 nanoparticles, a superhydrophobic surface can be realized.[13,26–28] It is because that, to acquire a superhydrophobic surface, both low-surface energy substance and micro–nano-binary scale surface roughness are required according to research reported previously.[29,30] The selective wettability and permeability of the honeycomb coating layers allow the porous composite to be directly used as an oil–water separator.

A cellulose-based filter paper is hydrophilic, economic and accessible. As a filter material, the large pore volume and high filtration efficiency ensure their direct use for oil/water separate filtration, only after being endowed with selective wettability. Herein, we first present a BF lithography-based strategy for *in situ* generating selective wettable coating layers on filter papers, the obtained composites may directly apply to oil–water separation. A comb-like fluorine-containing amphiphilic polymer denoted as PBTF-*X* (*X* represents the percentage of the monomer units equipped with hydrophilic side chains in total monomer units (%)) was employed in the BF process with the aim of generating a kind of coating layer on filter papers, which possess both the permeable honeycomb morphology and selective wettability introduced by the low-surface free energy substance. By regulating the PBTF solution concentration and the hydrophilic side chain density of PBTF, hydrophobic honeycomb coating layers (WCA = 146°) were obtained, which contour to the profile of the filter paper. According to SEM analysis, the coating layers formed by PBTF-50 show multilayer porosity, ultrathin polymer skeletons between two spherical cavities as well as high cavity volume proportion, which imply the high content of the internal water phase in the PBTF-50 solution during the BF process. Inspired by this, the PBTF-50 dichloromethane solution was premixed with an appropriate amount of water, and the formed nano-emulsion was applied in the BF process. According to the SEM analysis, a coating layer with micro–nano-sized communicating pores was uniformly formed on the surface of the filter paper. The as-obtained PBTF coated filter paper exhibits superhydrophobic property with a WCA of 152°, which guarantees its high separation efficiency during the oil/water separation process.

Experimental

Materials

Trans-1,4-Polybutadienes (TPBs, M_n = 32.4 kg mol^{-1}, M_w/M_n = 1.56, *trans*-1,4 content ≥95%, laboratory-made), *m*-chloroperoxybenzoic acid (*m*-CPBA, 85%), *m*-(trifluoromethyl)phenyl isocyanate (TFPI, 96%), tin(II) 2-ethylhexanoate (97%), chloroform-d (99.8 at%), 1,2-dichlorobenzene-d^4 (99.5 at%), superdry methyl alcohol (99.9%), petroleum ether (99.9%) and HCl (36.7%) were purchased from Aladdin. All of above-mentioned chemicals were used as received without further purification. Toluene, superdry dichloromethane (DCM) and tetrahydrofuran (THF) were purified by a standard method and stored in nitrogen atmosphere. A qualitative filter paper with a pore size of 20 μm was purchased from New Star Company. A syringe filter (Nylon 66 membrane) with a pore size of 0.45 μm was purchased from Jing Teng Company.

Preparation of PBTF-*X*

PBTF-*X* was prepared according to the procedure reported previously.[31]

Preparation of PBTF-*X*-coated filter papers by the BF process

The preparation process of PBTF-*X* honeycomb membranes is as follows: PBTF was first dissolved in DCM and a transparent solution (10 mg mL^{-1}) was formed. The solution was casted onto a piece of filter paper at room temperature of 25 °C with moisture supplied by an inverted funnel under the flow of gas over the substrate with a relative humidity (RH) of about 60% at

a flow rate of 1.0 L min^{-1}. The honeycomb coating layers were formed *in situ* on the surface of the filter paper within 10 minutes.

Preparation of the nano-emulsion

Take PBTF-50 as an example. First, 5 mL of PBTF-50 in the DCM solution (10 mg mL^{-1}) was mixed with 2 μL distilled water, and the mixture was applied to ultrasonic concussion for 5 minutes and then filtered using a syringe filter (0.45 μm pore size). The obtained translucent nano-emulsion (N-50) was used for the TEM and DLS experiments. The nano-emulsions applied in the BF process with different water contents (2 μL, 5 μL and 10 μL) were prepared in the same way except that the filtration step was excluded.

Preparation of nano-emulsion-coated filter papers by the BF process

A piece of neat filter paper was dipped into the as-prepared nano-emulsion for 5 seconds and then taken out for the above-described subsequent BF process, with all the physical conditions kept constant.

Preparation of PBTF-*X*-coated filter papers *via* spin-coating

The preparation process of PBTF-*X* membranes on the filter paper is as follows: PBTF was first dissolved in DCM and a transparent solution (10 mg mL^{-1}) was formed. The solution was casted onto a piece of rotating filter paper at 25 °C, and the rotation speed was set at 1000 rpm with a spin time of 30 seconds. The obtained composites were dried at room temperature for 12 hours before the SEM measurement. Spin coating equipment KW-4A was produced by the Institute of Microelectronics, Chinese Academy of Sciences.

Oil/water separation

The as-prepared filter paper was used to separate a mixture of water and petroleum ether (v/v, 1/1). For visualization, water was dyed into light green and petroleum ether was dyed into pink. The mixture was separated using the device depicted in Fig. 10, and each phase was weighed separately. The separation efficiency was determined according to eqn (1):

$$\eta_{oil} = \frac{m_{oil}}{m_0} \times 100\% \quad (1)$$

In eqn (1), m_0 and m_{oil} are the masses of petroleum ether before and after the separation process.[32]

The flux (F) of the petroleum ether/water mixture was assessed by measuring the time spent in collecting the permeated oil and calculated using eqn (2):[33]

$$F = \frac{V}{St} \quad (2)$$

In eqn (2), V is the volume of petroleum ether, S the effective surface area of the superhydrophobic composite, and t the time.

Characterization

The ^{1}H NMR spectra of the samples were recorded using a Varian Unity 400 MHz spectrometer, with tetramethylsilane (TMS) as an internal standard, chloroform-d as the solvent in the room temperature test, and 1,2-dichlorobenzene-d^4 as the solvent in the variable temperature test. The nano-emulsion for the variable temperature test was prepared as follows: 5 mL PBTF-45 solution was mixed with 5 μL distilled water and then applied to ultrasonic concussion for 5 minutes. After filtration using a syringe filter (0.45 μm pore size), a translucent nano-emulsion was obtained.

The surface morphology of coating layers was characterized using a field emission scanning electron microscope (FESEM, XL-30 ESEM) at an accelerating voltage of 10 kV. The samples were sprayed with a layer of carbon before observation. The surface elemental composition mapping was obtained by energy-dispersive X-ray spectrometry (EDS, X-MAX Oxford Instrument Germany).

Transmission electron microscopic (TEM) images were recorded using a JOEL JEM-1011 instrument at an accelerating voltage of 100 kV. For TEM measurements, the solution and nano-emulsion were cast directly onto the surface of distilled water. The solution spread on the surface of water and evaporated into the membrane. The membrane was picked up by a copper grid and dried in an oven at 50 °C for 24 hours and then applied for the TEM test.

DLS measurements were recorded using a Brookhaven Nano Brook, particle/protein size and zeta potential analyzer equipped with a multi-digital time correlation instrument and a 35 mW He–Ne laser (λ = 632.8 nm) at an angle of 90°, with K = 1.868 × 105 cm^{-1}. The result was calculated using the most significant digit (MSD) algorithm, and the profile was taken from the intensity weight.

The surface tension was measured by OCA 25 (Data Physics, Germany) at room temperature by a hanging-drop method and calculated *via* digital image processing by the OWRK method. The water contact angle (WCA) of water droplets on the polymer films was measured using the same instrument. A water droplet (2 μL) was casted onto the sample, and the CA can be obtained by analyzing the shape of the water droplet. To minimize measurement errors, all of the CA data were averaged from five measurements for each sample at different positions. The dynamic sliding angle water droplet of size around 4 μL was recorded by the video mode.

Results and discussion

Amphiphilic characteristics of PBTF solutions

In the BF process, the orderly arrayed water droplet template is the guarantee for the generation of high-quality honeycomb membranes. The amphiphilic polymer molecules with the inherent affinity to water generally tend to assemble at the water/solution interface. The polymer aggregates and forms a protective layer around the water droplet and subsequently stabilizes the water droplet template, and thus, facilitates the formation of honeycomb membranes with highly regular

pores.[34] We have previously demonstrated PBTF material to be possessing internal physical crosslink networks that are composed of internal hydrogen bond donors and acceptors in solid state,[31] and now the property of PBTF in DCM solution is further explored. The chemical structure of PBTF-30 was first verified by ^{1}H NMR, and the spectrum is represented in Fig. 1, from which all the resonance signals belonging to the protons on the side chain can be clearly identified. The groups that serve as hydrogen bonding donors and acceptors in solid state and probably also involve in hydrogen bonding formation in solution state are colored and highlighted accordingly. Regardless of the actual bonding atoms and the complex bonding parameters of hydrogen bond in the solution state, with these potential hydrogen bond donors and acceptors on its side chain, PBTF can be functioned as an amphiphilic polymer and its DCM solution should exhibit amphiphilicity. As the interfacial tension test proved (ESI Fig. S1†), the interfacial tension between the PBTF-30 DCM solution and water was measured as 5.36 mN m^{-1}, which is much smaller than the interfacial tension between the pure DCM and water (28 mN m^{-1}). Such a sharp decrement in the interfacial tension originated from the aggregate of PBTF at the interface of the organic solvent and water through the formation of multiple hydrogen bonds with water molecules. Therefore, the PBTF DCM solution with confirmed amphiphilicity was employed in the BF process for the purpose to stabilize water droplets to facilitate the formation of honeycomb coating layers.

Effects of the solution concentration on the surface morphology

When the BF process was conducted on planar substrates, the micro-structures of honeycomb membranes can be influenced by various chemical and physical parameters. Changing the planar substrate to the bumpy filter paper will further complicate the situation. The uneven surface of the filter paper can be regarded as a chorography with "mountains" and "valleys". Once the solution is dropped onto the surface of the filter paper, it flows to the low-lying "valleys" under the action of gravity, which causes difference in the actual amount of the solution in micro-areas of the filter paper. As the solvent evaporates, the sequence of solution plasticization is from "mountains" to "valleys". Owing to the changes in the solution concentration introduced by solvent evaporation, a concentration gradient will be created, which is in contrast to the altitude of micro-areas. Since the solution concentration plays a positive role in stabilizing water droplets, and the morphology of pores is strongly affected by the water droplet template, it can be speculated that, at the end stage of the plasticization, the polymer solution in "valleys" micro-areas is in the semi-dry state but still deformable, while the plasticization of the solution in "mountains" has already been accomplished. The solutions in "valleys" with a higher concentration than those in "mountains" can stabilize the water droplet templates in much smaller size. Therewith, the final polymer coating layers are able to contour to the bumpy substrate and exhibit pore morphology in trends of large to small from "mountains" to "valleys". As a significant parameter in the BF process, the polymer solution concentration was first evaluated in order to obtain an optimum concentration before conducting the following investigations. PBTF can be well dissolved in DCM at different concentrations, which allows for the preparation of different micro-patterns. As shown in Fig. 2, some irregular open pores appeared on the surface of upper fibres with a pore size of *ca.* 2 μm when a concentration of 5 mg mL^{-1} was employed (Fig. 2(a)). In such a figure, it seemed that there were still some water droplets stabilized by the amphiphilic polymer, despite the relatively low solute content. However, due to the low concentration of a dilute solution, the polymeric protective layers around water droplets were too weak to stop these droplets from coalescing, which eventually led to large open pores with inconsistent sizes. Since the micro surface of the filter paper showed great unevenness, the amount of polymer solute introduced by the solution at a concentration of 5 mg mL^{-1} was inadequate for the construction of continuous polymeric coating layers. Single or multi-polymer-filaments could be found crossly suspending over the furrows formed by large height differences (Fig. 2(a)). Further increasing the polymer concentration to 15 mg mL^{-1} would endow the filter paper with a continuous honeycomb coating layer, which was contouring to the bumpy surface profile of the filter paper even in the deep furrows. The locally regular honeycombs with hexagonally packed frameworks and cyclic open pores indicated that the PBTF-30 could effectively stabilize water droplets, as highlighted in Fig. 2(b); therefore, the concentration of 15 mg mL^{-1} was suitable for the manufacture of PBTF honeycomb coating layers. The pore size in different micro-areas showed significant distinction, which was mainly derived from the complex surface topography of the filter paper. Slight differences in the depth of furrow or the

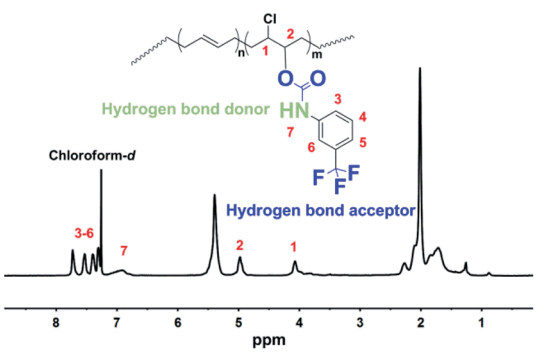

Fig. 1 ^{1}H NMR spectra of PBTF-30 in chloroform-d.

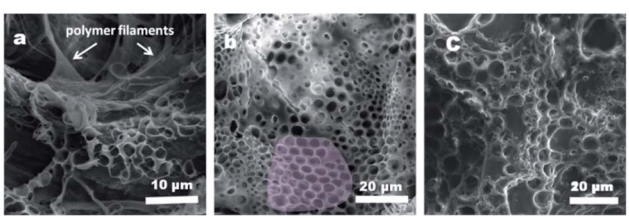

Fig. 2 SEM images of PBTP-30 micro-patterns formed at different concentrations: (a) 5 mg mL^{-1}; (b) 15 mg mL^{-1}; (c) 30 mg mL^{-1}.

angle of the micro-area orientation would influence the physical parameters actual acting on micro-areas during the BF process and result in different pore sizes and porosity. Increasing the polymer solution concentration to 30 mg mL^{-1} would result in a more viscous solution, which effectively prevented the water droplets from sinking and lead to the pores with dead ends. Moreover, the viscous solution would lengthen the water droplet residence time on the solution surface and make the water droplets coalesce;[35] the polymer coating layers taking these coalesced water droplets as templates would generate large pores with irregular pore size.

Effects of the polymer hydrophilic side chain density on the morphology and wettability of coating layers

Changing the side chain density can flexibly adjust the hydrophilicity of PBTF, and suitable hydrophilicity is the precondition for the formation of highly ordered BF arrays. Therefore, a range of PBTF-*X* (X = 10, 30, and 50) were synthesised and dissolved in DCM, and a solution with the optimal concentration of 15 mg mL^{-1} was formed. These solutions were utilized in the BF process in order to clarify the effect of polymer hydrophilicity on the morphology and wettability of the formed coating layers. As shown in Fig. 3(a), the formed coating layers fully covered the surface as a result of the appropriate solution concentration. With low hydrogen bond donor and acceptor contents, PBTF-10 appeared powerless in stabilizing the condensed water droplets, which yielded the polymer solution taking coalesced water droplets as templates, and resulted in coating layers with irregular pore shapes. Continuous honeycomb micro-patterns were obtained with local regularity on the surface of the filter paper in the case of PBTF-30, as specially marked out in Fig. 3(b). These honeycomb coating layers fully covered on the surface even including the deep furrows (ESI Fig. S2†). The diameter of open pores located on the upper fibres ranged widely from 5 μm to nearly 20 μm, while the denser pores formed in deep furrows exhibited honeycomb characteristics, which also had a wide range but much smaller pore size when compared to the pores located on upper fibres. Once being casted on the filter paper, the polymer solution would be spread out on the surface, which flowed into the furrows instantly, and the remaining bits of a solution on the upper fibres were subjected to more direct blowing of the airflow, which could accelerate the condensation of water vapor. The water droplets that acted as templates coalesced at a faster rate and some were deformed from a spherical to elliptical shape by the directional airflow, as depicted in Fig. 3(b). Since the morphology of honeycomb coating layers on the filter paper was affected a lot by the uneven substrate surface, the comparison of the pore size and porosity in different regions of honeycomb coating layers is meaningless. However, the honeycomb coating layers with pore size ranging from 200 nm to 600 nm were formed by taking PBTF-50 as the solute, which was significantly smaller than the size of the pores formed by PBTF-30 (Fig. 3(c)). The PBTF-50 polymer with abundant hydrogen bond donors and acceptors on its side chains had a strong tendency to form hydrogen bonding association with water molecules. The polymer aggregates at the interface of water and solvent caused a reduction in the interfacial tension between them, resulting in a growing interfacial area, an increase in the number of water droplets and a decrease in pore size.[36] By taking these water droplets as a template, the solute was able to form polymer honeycomb coating layers with nano-sized pores. A few rounded or irregular low-lying micro-areas with a pore size of *ca.* 1 μm were found in the continuous honeycomb layers, as shown in the highlighted area in Fig. 3(c).

More information on the morphology can be obtained from the enlarged SEM image (Fig. 4(a)). The explanation for the formation of such bumpy morphology was that, after most of the solvent evaporated, the polymer solution turned into a semi-solidified form with the order water droplet array inlay in it. The evaporation of the residual solvent would cause further condensation of water droplets onto the surface of the semi-solidified solution; the surface of the semi-solidified solution acted as an elastic net and the first layer of water droplets acted as a grid mesh. The newly generated water droplets were stabilized by the semi-solidified solution. These droplets rested on the semi-solidified solution and attempted to sink driven by gravity. Eventually, the semi-solidified elastic net was elongated by the concentration of stress, which formed pores o.d. gradually increasing size from top to bottom. Therefore, the coating layers were secondarily constructed, and a bumpy honeycomb

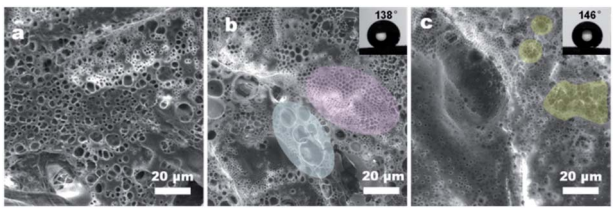

Fig. 3 SEM images of coating layers formed by PBTF-10 (a), PBTF-30 (b) and PBTF-50 (c).

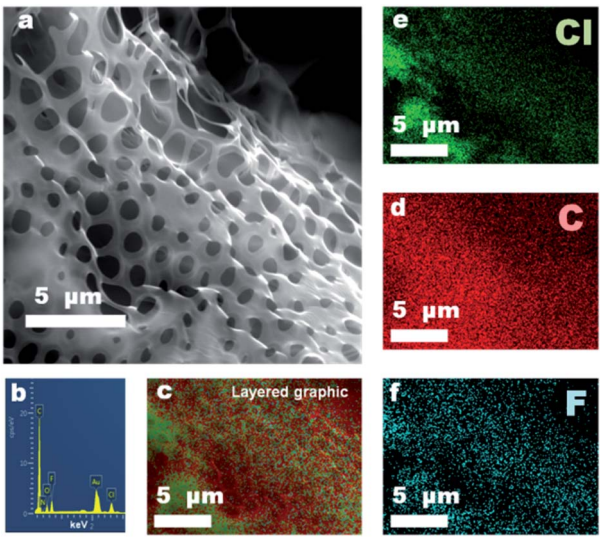

Fig. 4 Enlarged SEM images (a) and EDS mapping images (b–f) of honeycomb coating layers prepared by PBTF-50.

coating layer with nano-sized pores and micro-sized fluctuations was formed. The EDS images demonstrated that the coating layers with the secondarily constructed bumpy morphology were composed entirely of PBTF-50, without any additional material (Fig. 4(b–f)). The regional multilayer porosity was also found in the PBTF-50 coating layers. The embedded pores underneath the upper layer formed black circular shadows and arrayed orderly, and these shadows could be seen due to the ultrathin upper layer. According to the equation proposed by Bolognesi *et al.*[37] (ESI Fig. S3 and eqn S1†), the interfacial energy between the water droplets and the organic solvent was the main factor in determining the number of layers. The reduction in interfacial tension between the polymer solution and water droplets would accelerate the water droplets against the buoyancy to immerge into the viscous solution and form multilayer membrane. As the hydrophilicity increased with the hydrophilic side chain density of PBTF, from PBTF-10 to PBTF-50, there was a decreased tendency in interfacial tension between the polymer solution and water droplets, which originated from the increasing number of hydrogen bonds formed between amphiphilic polymers and water molecules. This probably explained the formation of multilayer porosity observed in the PBTF-50 solution. It is worth noting that multilayer and locally low-lying bumpy monolayer porosity simultaneously appeared on one sample, which implied the different physical parameters acting on micro-areas of the uneven substrate during the BF process, which led the different micro-areas of coating layers with not exactly the same but a quite similar morphology. PBTF-30 and PBTF-50 with the porous morphology can afford the roughness to endow the coated filter paper with hydrophobicity, in a manner similar to the topography of natural materials.[38,39] The WCA test was carried out and the coated surface showed WCAs of 138° and 146° respectively, as shown in the inset of Fig. 3(b) and (c). The smooth polymer coating layers formed by the spin coating method contribute a WAC of 116° on a planar glass slide and a WAC of 125° on a filter paper surface respectively (ESI Fig. S4†). The relatively large WAC of 138° that was obtained by conducting the BF process on the filter paper with the same polymer solution is presumably caused by the porous morphology, which contributes to the roughness and endows the coating layers with better hydrophobic capacity.

Characterization of nano-emulsions

The thin polymer coating layers made from PBTF-50 possessed nano-sized pores and extremely thin polymer partitions between the pores. Such ultrathin polymer skeletons between spherical cavities and the high cavity volume proportion in the coating layers implied the high-level stabilization of water droplets during the solidification process of the solution. These amphiphilic-molecule-protected water droplets on the surface of the polymer solution actually comprised a two-dimensional emulsion. The multilayer porosity observed in the PBTF-50 solution reminded us of a stable three-dimensional emulsion. Inspired by this, we premixed the PBTF-50 DCM solution with moderate distilled water. The well-dissolved polymer solutions were totally transparent to the eye, but when mixed with water, it became cloudy and displayed a strong Tyndall effect under the 405 nm ultraviolet light (ESI Fig. S5†). We speculated that the high hydrophilicity of PBTF-50 endowed the polymer solution with the ability of stabilizing micro–nano-sized water droplets and resulted in a nano-emulsion. In this way, a hydrogen bonding between amphiphilic polymers and water molecules in nano-emulsion was expected. By utilizing the sensitivity of hydrogen bonds to temperature, the existence and species of hydrogen bonding in PBTF-45 could be verified from the variable-temperature ^{1}H NMR spectra (Fig. 5). As a weak intermolecular association, hydrogen bonds are generally more fragile than other bonds and will certainly take the lead in breaking when the temperature rises. Therefore, the active proton on N–H groups will be released from the hydrogen bonding state and recover its extra-nuclear electron cloud density as well as its shielding effect, and thus, causes a shift of signal towards the high magnetic field, while other signals remain at the initial position. As the red arrow in Fig. 5 indicates, the resonance signal of proton located at 6.9 ppm shows a great temperature dependency, which indicated heat-induced disassociations of intermolecular hydrogen bonds. Another signal located at 10.95 ppm shows the same temperature dependency as the proton in the hydrogen bonding state, despite the puniness of the signal strength (Fig. 5 green dotted line position). The existence of two temperature-influenced signals gave a solid proof for the existence of two species of intermolecular hydrogen bonds. The signal at 6.9 ppm could be assigned to the hydrogen-bonded proton on –NH groups, where the tested solution is water free.[31] Another signal located at 10.95 ppm implied that there was a strong electron-withdrawing atom, which pulled the electron cloud around it and displayed a powerful de-shielding effect on the proton. Combining the strong electronegativity of oxygen in water molecules with the cloudy appearance of the tested PBTF-45 1,2-dichlorobenzene-d^4 solution, the signal in 10.95 ppm was assigned to the proton on N–H groups, which was in a hydrogen bonding state with the oxygen from water molecules. Increasing the hydrophilic moiety content would endow the PBTF with a high affinity to water. The

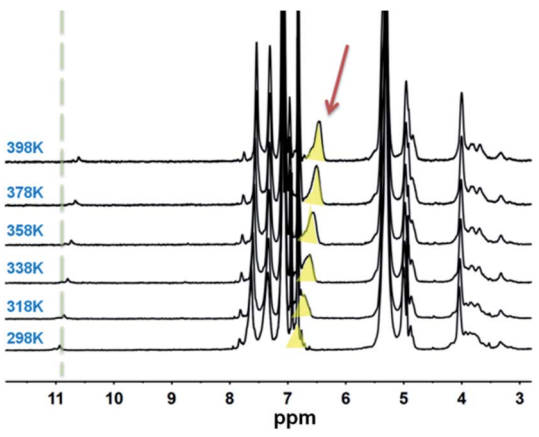

Fig. 5 Variable temperature ^{1}H NMR spectra of N-45 in 1,2-dichlorobenzene-d^4.

hydrogen bonding donors could be freely associated with the different acceptors. The intermolecular hydrogen bonding first formed between the PBTF-45 macromolecules, and then with surplus hydrogen bond donors, the hydrogen bonding between PBTF-45 macromolecules and water molecules took place. It is notable that the signal at 10.95 ppm did not show up till the hydrophilic side chain-equipped monomer unit content reached 40% of the total monomer units. When the modification degree of *trans*-1,4-polybutadienes is lower than 40%, the density of modification-introduced hydrogen bond donors and acceptors in the solution is too low (solution concentration = 5 mg mL^{-1}), the lack in the amount of hydrogen bond donors and acceptors reduces the possibility of their bonding with water molecules. Even if there are transient hydrogen bonds formed between PBTF and water, it is hard to be detected by ^1H NMR for the low hydrogen bond concentration.

To further clarify the aggregation state of water droplets in nano-emulsions, TEM and DLS experiments were conducted (Fig. 6 and 7). The prepared membranes were picked up by the copper grid without any special staining. Therefore, the contrast observed in images was due to the diffraction and phase contrast of the samples themselves. A close examination showed that PBTF-50 exhibited obvious micro phase separation due to the thermodynamic incompatibility of the hydrophilic and hydrophobic segments. The hydrophilic side chains in PBTF-50 aggregated *via* hydrogen bonding turned out to be spherical mono-disperse micelles with a diameter of 25 nm, while the DCM-soluble hydrophobic segment formed the continuous dispersion phase (Fig. 6(a)).

The TEM experiment of nano-emulsion N-50 was conducted, and the result is shown in Fig. 6(b). The hydrophilic sphere micelles were surrounded by corona, which formed the so-called core–shell structure. The diameter of the hydrophilic core ranged from 30 nm to 160 nm, and the corona shell showed non-uniform thickness. Compared with Fig. 6(a), the dark cores of the micelles were grown significantly in volume, and showed polydispersity. The uneven thickness of coronas indicated the different hydration levels of the hydrophilic cores, which were random and dynamic. There were fully hydrated hydrophilic cores that could not maintain the densely packed sphere shape but formed inverse micelles with irregular "water pool" appearance, which gave a visualized proof to the existence of nano-size stabilized water droplets. The nano-emulsion N-50 was put in a sealed vial and quiescence under 25 °C for 3 days, and no significant stratification or precipitation arose, which indicated that N-50 was in a meta-stable state. The TEM results were further confirmed by the DLS measurements (Fig. 7). After the addition of a moderate amount of water (2 μL), an increase in the hydrodynamic diameter of micelles from 28.1 nm to 39.2 nm was detected, where the hydrodynamic diameter that resulted from DLS measurements was slightly greater than the actual diameters of the micelles, as observed in TEM images (Fig. 6). The micelles with high light scattering intensities in the diameter size of 152.7 nm were also detected, which corresponded to the inverse micelles formed by fully hydrated hydrophilic segments.

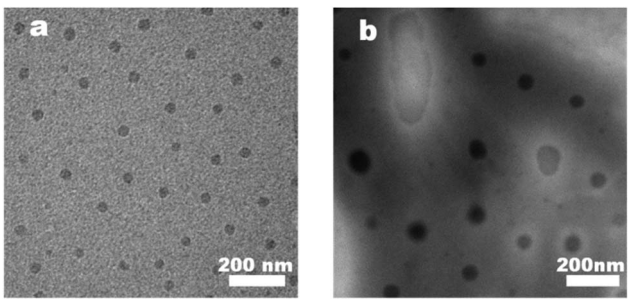

Fig. 6 TEM images of PBTF-50 (a) and nano-emulsion N-50 (b).

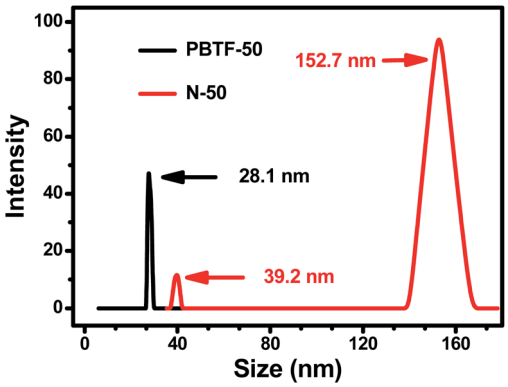

Fig. 7 Size distributions of PBTF-50 and N-50 based on DLS measurements.

Morphology of coating layers formed by nano-emulsions

Suffering from the unevenness of the filter paper substrate, the honeycomb membrane with perfect uniform porosity and surface wettability is difficult to be produced from a homogeneous polymer solution by the conventional BF process; therefore, the "generalized" BF methods are needed. The "generalized" BF method can produce honeycomb membranes, in which the water droplet templates are not only generated from water vapor, but also introduced by other ways, such as the water droplets in water-in-oil micro-emulsions.[40–42] Therefore, N-50 nano-emulsions with different water contents were utilized in the generalized BF process and a series of bird-nest-like micro-patterns with a hierarchical porous morphology were obtained instead of the honeycomb micro-patterns. An increase in the size of inverse micelles, as well as the forming pores, was observed as the water content increased; the pore size increased in the lower internal pores and the upper pores simultaneously, whereas the continuity of coating layers was decreased, as displayed in Fig. 8(a–d). The porous structure was further clarified from a high-magnification SEM image of Fig. 8(a), as shown in Fig. 9. The porous micro-patterns uniformly coated on the surface of the filter paper can be seen. The micro-patterns were composed of polymer skeletons and inter-connected pores with a pore size widely ranging from 0.28 μm to 2.9 μm. Considering the high hydrophilicity of nano-emulsion and the continuous introduction of water droplets in the BF process, the reason for the formation of such special surface morphology is explained

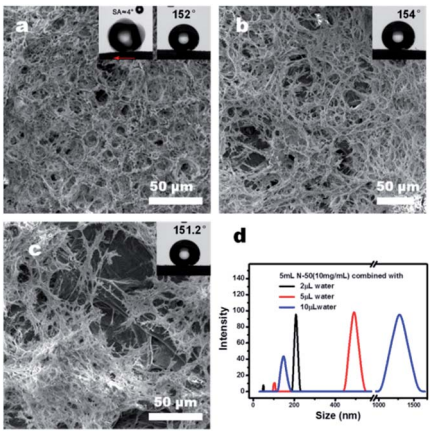

Fig. 8 SEM images of the coating layers formed by N-50 (5 mL, 10 mg mL^{-1}) with different water contents, 2 μL (a), 5 μL (b), and 10 μL (c) and the DLS curves of the corresponding nano-emulsions (d).

as follows: the hydrophilic nano-emulsion keeps absorbing the condensed water droplets during the BF process and intensifies the phase separation in nano-emulsions, and these water droplets will be dragged towards the bottom of the nano-emulsion by gravity and convection force in the same way as the case that happened in PBTF-50, but the difference is, these water droplets were dragged down and coalesced with the embedded water pools in N-50. As the solvent evaporation proceeds, the increase in the viscosity of the nano-emulsion will prevent the water droplets from sinking and let them stay on the surface of the nano-emulsion and then coalesce with each other. In the following polymer solidification, the nano-emulsion takes both enlarged internal water droplets and coalescing solvent vapour-induced water droplets as templates, leading to the formation of a hierarchical porous structure with communicating pores (Fig. 8(a)). The large-sized micelles in the nano-emulsion with high water content would result in discontinuous coatings (Fig. 8(c)). With the surface roughness endowed by the hierarchical porous morphology and the existence of fluorine as a low-surface energy substance, the coating layers may possibly generate superhydrophobicity. The speculation was confirmed by the WCA test. The N-50 nano-emulsion-coated filter paper showed a WCA over 150°, and a sliding angle of *ca.* 4; there is no obvious distinction in the surface wettability of the filter papers coated with nano-emulsions with different water contents, as shown in Fig. 8(a–c).

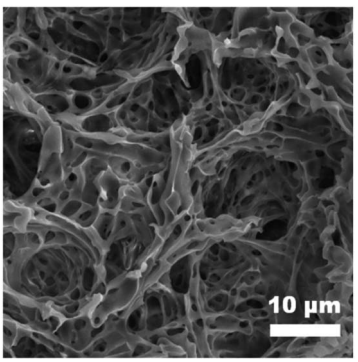

Fig. 9 High-magnification SEM image of the coating layers formed by N-50 (5 mL, 10 mg mL^{-1}) with 2 μL water.

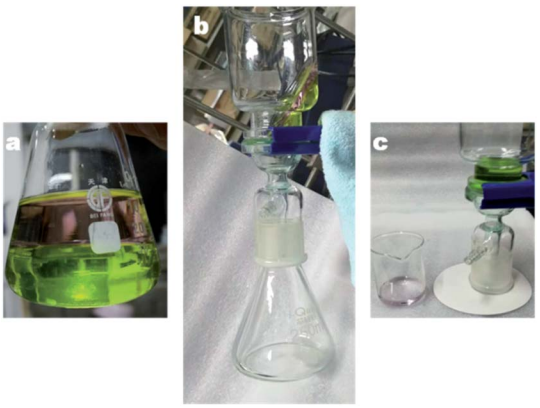

Fig. 10 Photographs of the oil/water separation process.

Oil/water separation by the N-50 coated filter paper

The N-50 nano-emulsion-coated filter paper with selective surface wettability and interconnected open pores (ESI Fig. S6†) can be readily utilized as an oil/water separation filter. As the WAC measurement shows, the N-50 coated filter paper reveals a WAC of 131° under the oil phase (ESI Fig. S7†). The satisfactory under-oil hydrophobicity ensures the reliability of the composites in oil/water separation. To evaluate the oil/water separation efficiency, a device was built, as shown in Fig. 10. For convenient visual distinction, petroleum ether was employed as the oil phase and dyed into pink, while water was dyed into light green. Petroleum ether is lighter than water and floats on water. The filtration was driven only by gravity. After filtration, the funnel was placed on a piece of filter paper for 2 minutes, and there was no color liquid dripped on the filter paper, which indicated the great separation efficiency. The exact separation efficiency was calculated using eqn (1), and the result is nearly 100%. (The video of the filtration process can be found in ESI Video 1.†) The flux (F) of N-50 (5 mL, 10 mg mL^{-1} with 2 μL water)-coated filter paper separator is 2989.15 L m^{-2} h^{-1}, as calculated using eqn (2). The data needed for the calculation were derived from ESI Video 2.†

Conclusion

A series of fluorine-containing amphiphilic polymer solutions have been employed to fabricate coating layers with various morphologies and wettabilities on a filter paper *via* a one-step low-energy consumption BF process. The effect of the solution concentration and the hydrophilic polymer side chain density on the honeycomb membrane morphology was studied in detail, and high-hydrophobicity polymer honeycomb coating layers that fitted the surface profile of the filter paper were obtained. Through further analysis, it was found that the PBTF-50 solution can stabilize interior nano-sized water droplets and

form a nano-emulsion, which was denoted as N-50. N-50 was applied in the BF process, and superhydrophobic coating layers with bird-nest-like micro-patterns were obtained continuously on the surface of the filter paper, and the formation mechanism of such micro-patterns was proposed. Equipped with the superhydrophobicity and the communicating pores, the N-50-coated filter paper turned into an oil/water separation filter, which was utilized in the separation of petroleum ether and water. The separation filter showed a separation efficiency as high as *ca*. 100%.

Conflicts of interest

There are no conflicts to declare.

Acknowledgements

This work was supported by Joint Funds of the National Natural Science Foundation of China (U1862206).

Notes and references

1 J. Aitkek, *Nature*, 1911, **86**, 516–517.
2 L. Rayleigh, *Nature*, 1911, **86**, 416–417.
3 G. Widawski, M. Rawiso and B. François, *Nature*, 1994, **369**, 387–389.
4 H. Ma and J. Hao, *Chem. Soc. Rev.*, 2011, **40**, 5457–5471.
5 U. H. F. Bunz, *Adv. Mater.*, 2006, **18**, 973–989.
6 M. H. Stenzel, C. Barner-Kowollik and T. P. J. Davis, *J. Polym. Sci., Part A: Polym. Chem.*, 2006, **44**, 2363–2375.
7 M. L. K. Hoa, M. Lu and Y. Zhang, *Adv. Colloid Interface Sci.*, 2006, **121**, 9–23.
8 M.-J. Chang, Y. Ai, L. Zhang, F. Gao and H.-L. Zhang, *J. Mater. Chem.*, 2012, **22**, 7704–7707.
9 Z. Dai, C.-S. Lee, B.-Y. Kim, C.-H. Kwak, J.-W. Yoon, H.-M. Jeong and J.-H. Lee, *ACS Appl. Mater. Interfaces*, 2014, **6**, 16217–16226.
10 R. Nagarale, G. Gohil and V. K. Shahi, *Adv. Colloid Interface Sci.*, 2006, **119**, 97–130.
11 T. J. Xu, *J. Membr. Sci.*, 2005, **263**, 1–29.
12 L.-S. Wan, J.-W. Li, B.-B. Ke and Z.-K. Xu, *J. Am. Chem. Soc.*, 2012, **134**, 95–98.
13 E. Bormashenko, S. Balter, Y. Bormashenko and D. Aurbach, *Colloids Surf., A*, 2012, **415**, 394–398.
14 P. Brown, E. Talbot, T. Wood, C. Bain and J. Badyal, *Langmuir*, 2012, **28**, 13712–13719.
15 X. Wang, Y. Pan, H. Yuan, M. Su, C. Shao, C. Liu, Z. Guo, C. Shen and X. Liu, *Chin. Chem. Lett.*, 2020, **31**, 365–368.
16 P. H. Tung, S. W. Kuo, K. U. Jeong, S. Z. Cheng, C. F. Huang and F. C. Chang, *Macromol. Rapid Commun.*, 2007, **28**, 271–275.
17 T.-Y. Zhang, L.-W. Mou, J.-Y. Zhang, L.-W. Fan and J.-Q. Li, *Int. J. Heat Mass Transfer*, 2020, **150**, 119352.
18 K. Li, X. Zeng, H. Li, X. Lai and H. Xie, *Mater. Lett.*, 2014, **120**, 255–258.
19 L. W. Wu, L. S. Wan, Y. Ou, L. W. Zhu and Z. K. Xu, *Adv. Mater. Interfaces*, 2015, **2**, 1500285.
20 L.-S. Wan, L.-W. Zhu, Y. Ou and Z.-K. Xu, *Chem. Commun.*, 2014, **50**, 4024–4039.
21 L.-S. Wan, J.-W. Li, B.-B. Ke and Z.-K. Xu, *J. Am. Chem. Soc.*, 2012, **134**, 95–98.
22 N. Noor, J. Koll, C. Abetz, H. Notzke and V. Abetz, *Sci. Rep.*, 2017, **7**, 1–9.
23 H. Ma, J. Cui, A. Song and J. Hao, *Chem. Commun.*, 2011, **47**, 1154–1156.
24 Y. Ou, C.-J. Lv, W. Yu, Z.-W. Mao, L.-S. Wan and Z.-K. Xu, *ACS Appl. Mater. Interfaces*, 2014, **6**, 22400–22407.
25 J. Mansouri, E. Yapit and V. Chen, *J. Membr. Sci.*, 2013, **444**, 237–251.
26 J. Zhang, Z. Meng, J. Liu, C. Schlaich, Z. Yu and X. Deng, *J. Mater. Chem. A*, 2017, **5**, 16369–16375.
27 X. Guan, J. Gong and B. Xu, *ACS Appl. Mater. Interfaces*, 2020, **12**, 17967–17978.
28 Q. Liu, Y. Wu and Z. Li, *Prog. Org. Coat.*, 2020, **149**, 105938.
29 T. Nishino, M. Meguro, K. Nakamae, M. Matsushita and Y. Ueda, *Langmuir*, 1999, **15**, 4321–4323.
30 L. Feng, Z. Zhang, Z. Mai, Y. Ma, B. Liu, L. Jiang and D. Zhu, *Angew. Chem., Int. Ed.*, 2004, **116**, 2046–2048.
31 X. Zhang, G. Sun and X. Zhang, *RSC Adv.*, 2020, **10**, 9387–9395.
32 C. Dai, N. Liu, Y. Cao, Y. Chen, F. Lu and L. Feng, *Soft Matter*, 2014, **10**, 8116–8121.
33 Q.-Y. Cheng, C.-S. Guan, Y.-D. Li, J. Zhu and J.-B. Zeng, *Cellulose*, 2019, **26**, 2861–2872.
34 B.-B. Ke, L.-S. Wan, W.-X. Zhang and Z.-K. Xu, *Polymer*, 2010, **51**, 2168–2176.
35 E. Servoli, G. A. Ruffo and C. Migliaresi, *Polymer*, 2010, **51**, 2337–2344.
36 A. Chen, I. Blakey, A. K. Whittaker and H. J. Peng, *J. Polym. Sci., Part A: Polym. Chem.*, 2016, **54**, 3721–3732.
37 A. Bolognesi, C. Mercogliano, S. Yunus, M. Civardi, D. Comoretto and A. Turturro, *Langmuir*, 2005, **21**, 3480–3485.
38 J. Kamei, Y. Saito and H. Yabu, *Langmuir*, 2014, **30**, 14118–14122.
39 H. Yabu, M. Takebayashi, M. Tanaka and M. Shimomura, *Langmuir*, 2005, **21**, 3235–3237.
40 J. Liang, Y. Ma, H. Sun, W. Li and L. Wu, *J. Colloid Interface Sci.*, 2013, **409**, 80–87.
41 Y. Ma, J. Liang, H. Sun, L. Wu, Y. Dang and Y. Wu, *Chem.–Eur. J.*, 2012, **18**, 526–531.
42 B. You, L. Shi, N. Wen, X. Liu, L. Wu and J. Zi, *Macromolecules*, 2008, **41**, 9952.